

Chapter 2

The ATLAS Experiment at the Large Hadron Collider

The Large Hadron Collider (LHC) is the world's highest-energy particle accelerator, designed to collide protons at a center-of-mass energy of 14 TeV. The ATLAS experiment is one of the two multi-purpose experiments that take advantage of the collisions provided by the LHC. It has been conceived to pursue an ambitious physics program, where the first milestone was the discovery of the Higgs boson, achieved in 2012 [1, 2]. This chapter introduces CERN's accelerator complex and describes the main aspects of the ATLAS detector at the LHC.

2.1 The Large Hadron Collider

The Large Hadron Collider (LHC) [3] is a circular particle accelerator installed in a 27 km long underground tunnel, and designed to collide protons at a center-of-mass energy of $\sqrt{s} = 14$ TeV. On the accelerator ring four detectors (ALICE [4], ATLAS [5], CMS [6] and LHCb [7]) have been built around four different interaction points, to record and study the collisions delivered by the LHC. ATLAS and CMS are multipurpose experiments designed to study a broad range of physics processes. The LHCb experiment is specialized in the detection of b -hadrons, while the ALICE collaboration focuses on the study of heavy-ion collisions.

Since 2010, the LHC has delivered proton–proton (pp) collisions at a center-of-mass energies of 7 and 8 TeV (in 2011 and 2012, respectively), about half of its nominal energy. The LHC has produced also lead-ion (Pb–Pb) collisions with a per-nucleon center-of-mass energy of $\sqrt{s_{NN}} = 2.76$ TeV and proton–lead (p–Pb) collisions with $\sqrt{s_{NN}} = 5.02$ TeV.

The protons are accelerated to the desired energy through various steps. First, protons are extracted from the ionization of hydrogen gas and injected in the linear accelerator LINAC2, where they are accelerated to an energy of 50 MeV. They are

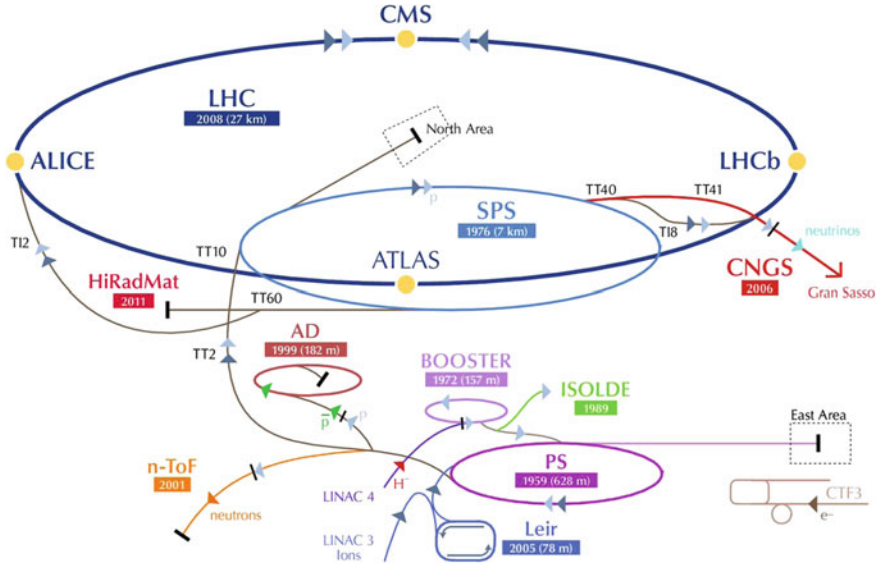


Fig. 2.1 Schematic view of the CERN accelerator complex. The four main LHC experiments are shown at the interaction points

then transferred into the Proton Synchrotron Booster (PSB) and accelerated up to an energy of 1.4 GeV. A second circular accelerator, the Proton Synchrotron (PS) brings the energy of the protons to 25 GeV before injecting them into the Super Proton Synchrotron (SPS). After being accelerated to 450 GeV, the protons finally enter the two LHC beam pipes where they are boosted to energies of up to 4 TeV. A schematic view of the acceleration chain is shown in Fig. 2.1.

Besides its high energy, the LHC also outperforms previous accelerators in the delivered luminosity. The instantaneous luminosity \mathcal{L} is defined as:

$$\mathcal{L} = \frac{n_b f_r n_1 n_2}{2\pi \Sigma_x \Sigma_y}, \quad (2.1)$$

where n_1 and n_2 are the bunch populations (number of protons per bunch) in beams 1 and 2 respectively, f_r is the revolution frequency of the LHC, n_b are the number of bunch pairs colliding in each revolution, and Σ_x and Σ_y characterize the horizontal and vertical convolved beam widths.

The event rate of a certain process can be obtained as the product of the process cross section and the instantaneous luminosity:

$$\frac{dN}{dt} = \mathcal{L} \times \sigma. \quad (2.2)$$

Table 2.1 Overview of the parameters for the LHC performance comparing the design values with their time evolution during the first long run operation in 2010–2013

Parameter	Design value	2010	2011	2012
Beam energy (TeV)	7	3.5	3.5	4
Beta function β^* (m)	0.55	2.0/3.5	1.5/1.0	0.6
Max. num. bunches/beam	2808	368	1380	1380
Max. num. protons/bunch	1.15×10^{11}	1.2×10^{11}	1.45×10^{11}	1.7×10^{11}
Bunch spacing (ns)	25	150	75/50	50
Peak luminosity ($\text{cm}^{-2} \text{s}^{-1}$)	1×10^{34}	2.1×10^{32}	3.7×10^{33}	7.7×10^{33}
Emittance ϵ_n (μrad)	3.75	2.0	2.4	2.5
Max. $\langle\mu\rangle$	19	4	17	37

The instantaneous luminosity at the ATLAS collision point is measured by dedicated subdetectors that are described in Sect. 2.3. In 2012, the LHC reached a peak luminosity of $7.7 \times 10^{33} \text{ cm}^{-2} \text{s}^{-1}$, which is more than half the design luminosity. Table 2.1 shows the relevant parameters for the accelerator performance.

Due to the high frequency of collisions and the high density of the bunches necessary to achieve such a high luminosity, there is a non-zero probability that several events, originating from different pp collisions, may occur simultaneously. These events are referred to as *pile-up* and are categorized as in-time or out-of-time pile-up. In-time pile-up events are caused by additional interactions of protons in the same bunch collision. The out-of-time pile-up occurs when traces from an event in a different bunch-crossing are recorded. The mean number of interactions per bunch crossing $\langle\mu\rangle$, which is taken as measure of the pile-up activity, is shown in Fig. 2.2a.

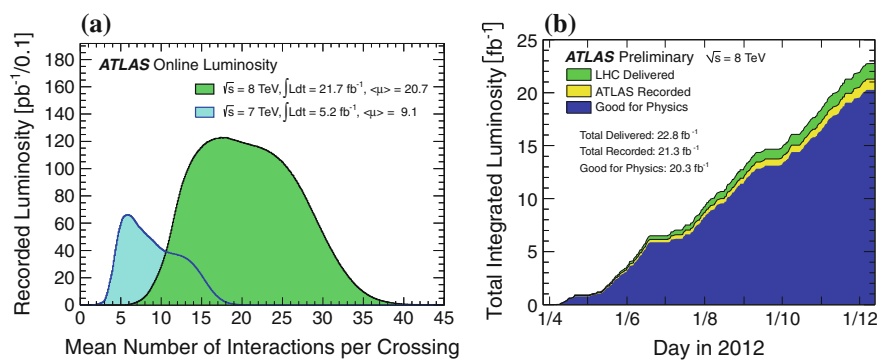


Fig. 2.2 **a** Mean number of interactions per beam crossing during the 2011 and 2012 LHC runs. **b** Total integrated luminosity versus time delivered by the LHC to ATLAS (in green), recorded by the experiment (in yellow) and selected as good data for analysis (in blue) for pp collisions $\sqrt{s} = 8 \text{ TeV}$ in 2012

Integrating the instantaneous luminosity over the accelerator active time (a “fill”, when stable beams are kept colliding) the integrated luminosity is obtained, relating the total number of produced events N_{tot} to the cross section:

$$N_{\text{tot}} = \sigma \int \mathcal{L} dt . \quad (2.3)$$

In 2010 ATLAS collected about 45 pb^{-1} of pp collision data at $\sqrt{s} = 7 \text{ TeV}$, and in 2011 it reached about 5 fb^{-1} at the same center-of-mass energy. During 2012, the last year of data taking before the long shutdown,¹ ATLAS collected about 20 fb^{-1} of pp collision data at $\sqrt{s} = 8 \text{ TeV}$. Figure 2.2b shows the luminosity recorded by ATLAS during stable beam conditions. The difference with respect to the delivered luminosity is due to Data AcQuisition (DAQ) inefficiencies. Of the recorded luminosity, only a part is usable for analysis, which is referred to as “good data”, i.e. the data that satisfy Data Quality (DQ) requirements assessed after reprocessing (see Sect. 2.5).

2.2 The ATLAS Experiment

ATLAS (A Toroidal LHC ApparatuS) [5] is a general purpose experiment aimed at exploring a vast range of physics scenarios and designed to measure the particles produced in pp collisions at the LHC at unprecedented energies and instantaneous luminosities. It is the biggest detector of its kind ever built (about 46 m long, 25 m wide and weights 7000t) and it is characterized by a full coverage of the space around the pp interaction point and complete containment of the particles produced in the collision. Different subsystems are layered concentrically one after the other, as shown in Fig. 2.3, each devoted to the measurement of different properties for different types of particles. The subdetectors are grouped into three main systems:

- The Inner Detector, immersed in a solenoidal magnetic field, constitutes a tracking system used to identify and measure the momenta of charged particles and to identify the interaction vertices and the displaced vertices.
- The Calorimeters are used to identify and measure the energy of neutral and charged particles. They are designed to stop most types of particles, except for muons and neutrinos.
- The Muon Spectrometer is used to detect and measure the properties of muons. Because muons minimally interact with the other parts of the detector and have long lifetimes, they are identified and measured in the outermost detector layer.

¹LHC terminated the first phase of the pp program at the end of 2012, operated proton-heavy ion collisions for two months at the beginning of 2013 and then stopped for what is called the first “long shutdown”. During these two-years the accelerator and the experiments underwent substantial maintenance and upgrade works, in order to be re-operated in 2015 with higher performance at a higher center-of-mass energy for particle collisions.

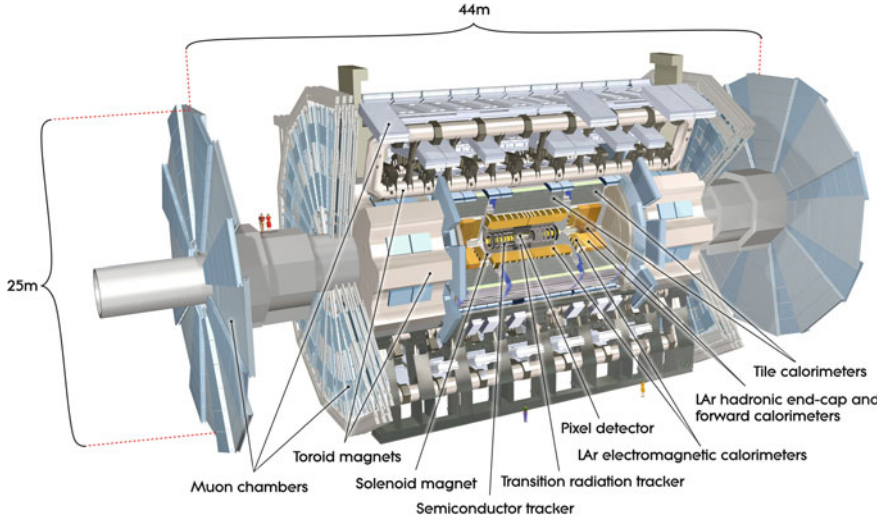


Fig. 2.3 Drawing of the ATLAS detector showing the different subdetectors and the magnet systems

2.2.1 Coordinate System

The ATLAS reference system is a cartesian right-handed coordinate system with origin at the nominal interaction point (IP) in the center of the detector. The X -axis points from the IP to the center of the LHC ring, the Y -axis points upwards and the positive Z -axis is defined along the anti-clockwise beam direction. The azimuthal angle ϕ is measured around the beam axis, ranging between $-\pi$ and $+\pi$ with respect to the X -axis. The polar angle θ is measured with respect to the Z -axis and ranges between 0 and π . Since the momentum of the colliding partons along the Z -axis is unknown, it is useful to define the transverse component of variables of interest, like energy and momentum, defined as the projection on the XY plane, which are boost-invariant along the Z -axis:

$$E_T = E \sin \theta, \quad p_T = p \sin \theta. \quad (2.4)$$

Another common variable used at hadron colliders to describe the polar distribution and preferred to the simple polar angle θ is the rapidity y :

$$y \equiv \frac{1}{2} \ln \left(\frac{E + p_z}{E - p_z} \right), \quad (2.5)$$

which, for vanishing particle mass, is equal to the pseudorapidity η :

$$\eta \equiv -\ln \left(\tan \frac{\theta}{2} \right). \quad (2.6)$$

The advantage of both variables over θ is that rapidity differences Δy are boost-invariant along the Z -axis, as well as pseudorapidity differences $\Delta\eta$ for massless particles. The pseudorapidity is usually preferred to the rapidity as it does not require knowing the particle's mass but only its polar position. The distance between two particles is often referred to in terms of ΔR :

$$\Delta R \equiv \sqrt{(\Delta\eta)^2 + (\Delta\phi)^2} . \quad (2.7)$$

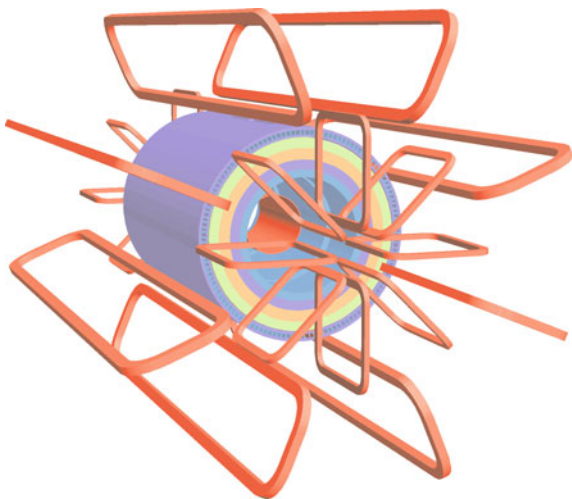
ATLAS covers the pseudorapidity regions up to $|\eta| < 4.9$. However, physics analyses typically consider objects restricted to the pseudorapidity region $|\eta| < 2.5$.

2.2.2 Magnet System

The measurement of charged particles' momenta is based on their deflection in a magnetic field. The magnet system [8] represents a particular characteristic of the ATLAS experiment which sets it apart in the panorama of high energy physics. It is composed of four large superconducting magnets designed to provide a field mostly orthogonal to the particle trajectory: a central solenoid and three open-air toroids as shown in Fig. 2.4.

The central solenoid surrounds the Inner Detector and provides a magnetic field parallel to the beam axis bending charged particles in the ϕ direction. At the interaction point the value of the magnetic field is 2T and it remains constant in the radial direction. As the distance from the interaction point increases in the z direction, the field strength decreases as a result of the finite size of the solenoid.

Fig. 2.4 Schematic view of the ATLAS magnet system: three external toroids and the central solenoid enclosed by the calorimeters



The toroid system produces the field needed by the muon spectrometer to deflect particles in the η direction: two end-cap toroids at the two extremes of the detector and a barrel toroid centrally located around the calorimeters. Each toroid is composed of eight independent coils equally distributed in the azimuthal plane. The barrel toroid generates a magnetic field of 3.9T while the end-cap produces a field of 4.1T. The choice of the “open air” toroid configuration was made to improve the muon reconstruction performance without relying on the Inner Detector. The toroids allow to efficiently generate the magnetic field over a large volume with a reduced amount of material. This minimizes the amount of multiple scattering,² which represents one of the factors limiting the muon momentum resolution.

2.2.3 Inner Detector

The Inner Detector (ID) [9] is the subdetector closest to the IP. It provides tracking of charged particles arising from collisions, allowing for vertex reconstruction and measurement of track momenta in the range $|\eta| < 2.5$. The detector design required fast response electronics, good radiation resistance and reducing to a minimum the amount of material to be placed in front of the calorimeters to avoid degrading the energy measurement. It is divided in three different concentric subdetectors, named (increasing in distance with respect to the IP) pixel, semi-conductor tracker (SCT) and transition radiation tracker (TRT). Figure 2.5 shows a cut-away view of the ATLAS ID.

2.2.3.1 Pixel

The pixel detector is the innermost part of the ID and measures charged particles using radiation-hard silicon sensors (pixels). It covers the region $|\eta| < 2.5$ and is composed of three cylindrical layers in the barrel region, and of three concentric discs in the end-cap region. Each silicon pixel has a size of $50 \times 400 \mu\text{m}^2$ and is $250 \mu\text{m}$ thick, resulting in total ≈ 80.4 million readout channels to achieve a very fine granularity. The precision is of $10 \mu\text{m}$ in the $R - \phi$ plane, and $115 \mu\text{m}$ in Z and R in the barrel and end-cap region, respectively. The very first layer is called B-layer and, thanks to its position really close to the IP, 50.5 mm away, allows for the reconstruction of secondary vertices associated with the production of long-lived particles such as b -hadrons. This information is very useful to identify jets originating from the fragmentation of b -quarks.

²Multiple scattering is defined as the electromagnetic interaction of a charged particle with the atomic structure of the medium. The result of the interaction with the very large number of nuclei and electrons results into a random smearing of the momentum of the incoming particle.

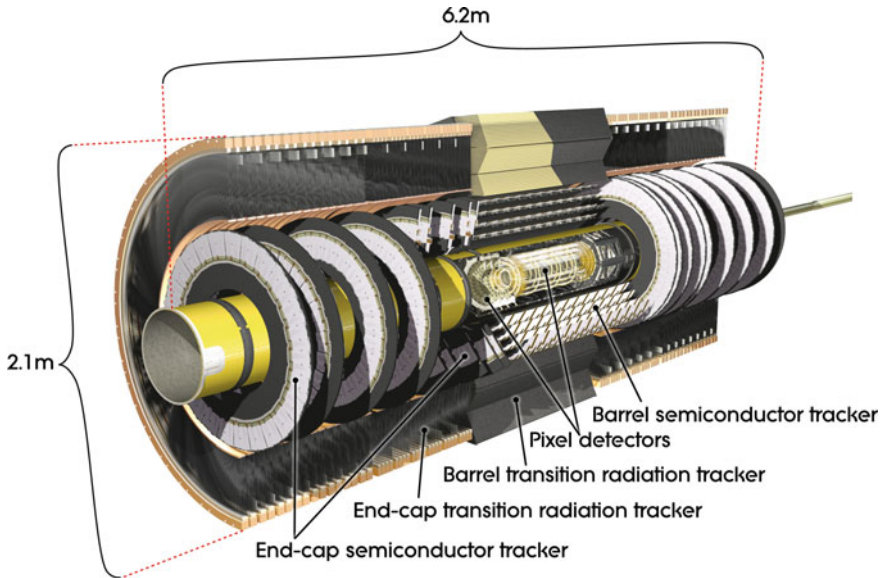


Fig. 2.5 Cut-away view of the ATLAS inner detector

2.2.3.2 Semiconductor Tracker

The Semiconductor Tracker (SCT) is the middle part of the ID and is a silicon microstrip detector. It is composed of a barrel, with four layers of silicon microstrip detectors, and two endcaps, each with nine disks, covering the range $|\eta| < 2.5$. The minimal SCT unit, the module, is a pair of single-sided silicon microstrip sensors mounted back-to-back, containing 768 microstrips. The back-to-back sensors are mounted with a 40 mrad “tilt” angle, so that the crossing point of the strips on both sides is used to determine the space point position. In the barrel, silicon strips are arranged parallel to the beam line, while in the disks, the strips are oriented radially. The spatial resolution achieved is $17\ \mu\text{m}$ in $R - \phi$ and $580\ \mu\text{m}$ in Z (R) in the barrel (end-cap) region.

2.2.3.3 Transition Radiation Tracker

The Transition Radiation Tracker (TRT) is the outermost part of the ID. It consists of 4 mm-diameter gaseous straw tubes interleaved with transition radiation material, enabling tracking for $|\eta| < 2$. The space between the tubes is filled with plastic material (polyethylene) in order to produce the transition radiation. The emission of photons depends on the Lorentz boost γ (E/m) of the particles and, in the energy range of interest, is present only for electrons. The TRT is only segmented in $R - \phi$, and it provides a resolution of $130\ \mu\text{m}$ per straw.

2.2.3.4 Inner Detector Combined Performance

The relative precision of the three subdetectors is comparable so that no single measurement dominates the momentum resolution.³ Using the combined information from the three subdetectors, the transverse momentum resolution measured with cosmic muons [10] is:

$$\frac{\sigma_{p_T}}{p_T} = 1.6 \% \oplus \frac{0.053 \%}{\text{GeV}} \times p_T, \quad (2.8)$$

This translates in a resolution of 1.6 % for tracks with $p_T \sim 1 \text{ GeV}$ and of about 50 % for $p_T \sim 1 \text{ TeV}$.

2.2.4 Calorimeters

The ATLAS calorimeters surround the ID, covering the full ϕ space and the range $|\eta| < 4.9$. They are designed to stop and contain most of the particles from the interaction, except for muons and neutrinos. The calorimeters are divided into a central barrel part and two symmetric end-caps, as shown in Fig. 2.6. In the acceptance

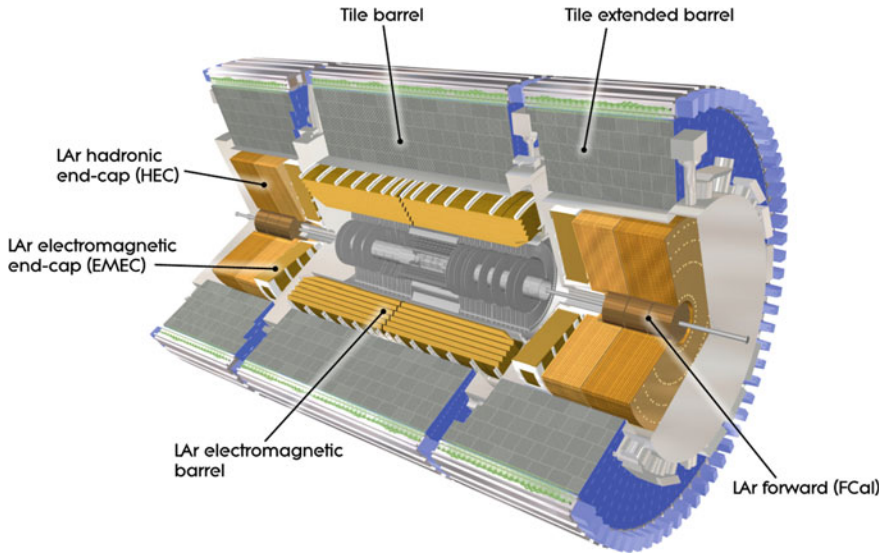


Fig. 2.6 Schematic view of the ATLAS calorimeter system

³The lower intrinsic resolution of the TRT is compensated by the higher number of hits per track and by the possibility of analyzing a longer track segment.

region covered by the ID the electromagnetic calorimeter has very fine segmentation for precise measurement of photons and electrons. The hadronic and forward calorimeters have coarser segmentation but still allow a precise measurement of jet kinematics as well as sufficient pseudorapidity coverage for the missing transverse energy calculation.

2.2.4.1 Electromagnetic Calorimeter

The electromagnetic calorimeter (ECAL) [11] is a sampling calorimeter that uses liquid argon (LAr) as active material and lead plates as absorber. The liquid argon solution was adopted for its intrinsic linear behavior, high ionization yield, stability and resistance to radiation. The lead plates have a characteristic accordion shape and are oriented in the radial direction. This allows a complete symmetric coverage without cracks in the azimuthal direction. High voltage is applied between absorber plates to collect the ionization electrons from the interaction in the liquid argon as well as to produce the signal amplification. The ECAL barrel covers the range $|\eta| < 1.475$, while the end-caps extend the reach to $1.375 < |\eta| < 3.2$.

The ECAL barrel is segmented in order to create three longitudinal sections with very different depths and cell structure in the $\eta - \phi$ plane. Figure 2.7a shows the geometry of one module of the calorimeter.

The first layer, with a thickness of 4.3 radiation lengths (X_0), is finely segmented in η with thin readout strips of $\Delta\eta \times \Delta\phi = 0.0031 \times 0.098$, in order to measure precisely the direction in pseudorapidity of the particles. The strip layer is of particular

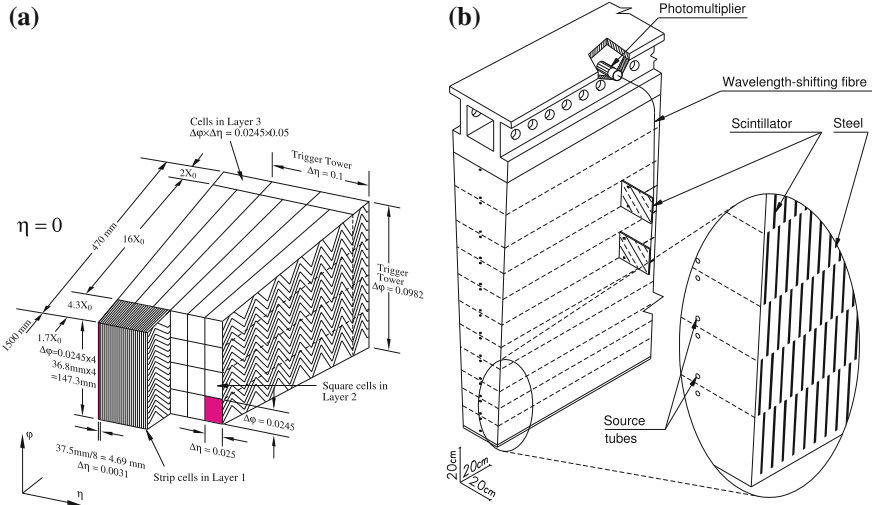


Fig. 2.7 Schema of different modules of the ATLAS calorimeters: **a** electromagnetic calorimeter and **b** hadronic calorimeter

importance for photon and electron identification and, combined with the information from the second layer, can be used to obtain precise information on the photon's production vertex. The second layer, $16X_0$ thick, represents most of the thickness of the calorimeter. It is divided in towers of size $\Delta\eta \times \Delta\phi = 0.025 \times 0.025$ and provides the position measurement of the cluster. About 95% of the energy of the shower is deposited in a matrix of 3×7 towers in $\Delta\eta \times \Delta\phi$. The third layer, just $2X_0$ thick, has coarser granularity and it is used to estimate the amount of energy lost beyond the ECAL. Towers in this region have a dimension of $\Delta\eta \times \Delta\phi = 0.05 \times 0.0245$. In the central region an additional pre-sampler layer is present. The information from this layer is exploited in the calibration to estimate the energy lost by the electron or photon in the passive material of the solenoid.

The total thickness of the ECAL is at least $22 X_0$, increasing with η from $22 X_0$ to $33 X_0$ in the barrel and from $24 X_0$ to $38 X_0$ in the endcap. This guarantees a full containment of electrons and photons up to energies of a few TeV.

The target energy resolution for the ATLAS electromagnetic calorimeters is [11]:

$$\frac{\sigma_E}{E} = \frac{10\%}{\sqrt{E}} \oplus \frac{17\%}{E} \oplus 0.7\% , \quad (2.9)$$

with E measured in GeV.

2.2.4.2 Hadronic Calorimeter

The ATLAS hadronic calorimeter is composed of different independent sampling calorimeters, each with its own particular technology and choice of material. The choice was dictated by the different conditions in terms of radiation flux and performance requirements as a function of the pseudorapidity of the particles.

In the central region the Tile Calorimeter [12], referred to as TileCal, covers the range $|\eta| < 1.7$. It consists of a sampling calorimeter employing steel tiles as passive material (absorber) and plastic scintillators as active material. Figure 2.7b shows a schema of one TileCal module. TileCal is divided into a long barrel (LB, $|\eta| < 1.0$) and two extended barrels (EB, $0.8 < |\eta| < 1.7$). Both the LB and the EB are segmented into 64 modules in ϕ , corresponding to a $\Delta\phi$ granularity of 0.1 radians. Radially, each module is further segmented into three layers, with thicknesses of approximately 1.5 , 4.1 and 1.8 hadronic interaction lengths (λ) for the barrel and 1.5 , 2.6 and 3.3λ for the extended barrel. The $\Delta\eta$ segmentation of each module is 0.1 in the first two radial layers and 0.2 in the third one.

Wavelength-shifting fibers coupled to the tiles on either ϕ edge of the cells collect the light produced and are read out by two photomultiplier tubes (PMT), each linked to one readout channel. The readout channels are grouped into cells forming a pseudo-projective geometry in η , as shown in Fig. 2.8.

The transition region between the LB and the EB is supplemented with a set of special cells: the gap scintillators cover the region of $1.0 < |\eta| < 1.2$ while the

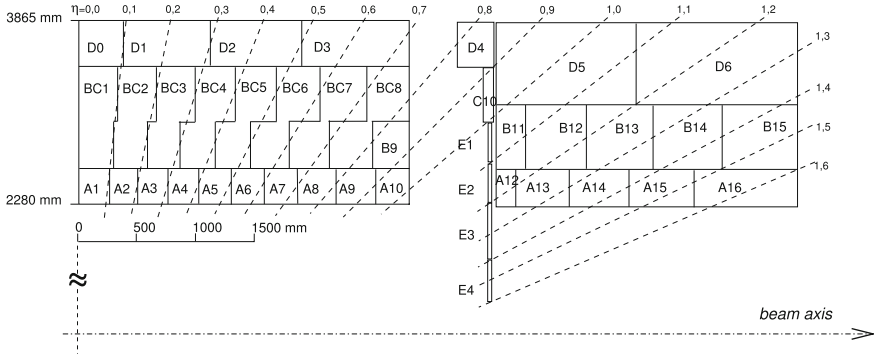


Fig. 2.8 Layout and geometry of the cells and layers in the hadronic calorimeter

crack scintillators are located on the front of the LAr end-cap and cover the region $1.2 < |\eta| < 1.6$.

The author has contributed to performance studies of the hadronic calorimeter, and the work has been documented in Appendix A.

The Hadronic End-Cap calorimeter (HEC) uses copper as passive material and liquid argon as active material, chosen for its radiation hardness in a region ($1.5 < |\eta| < 3.2$) exposed to a significant particle flux. Each HEC is composed of two independent wheels with granularity varying with η . In $1.5 < |\eta| < 2.5$, $\Delta\eta \times \Delta\phi = 0.1 \times 0.1$ in the first two longitudinal layers, and 0.2×0.1 in the last one. In the range $2.5 < |\eta| < 3.2$, the granularity is $\Delta\eta \times \Delta\phi = 0.2 \times 0.2$ in all the three samples.

Finally, the Forward Calorimeter (FCal) covers the very forward region of pseudorapidity, $3.1 < |\eta| < 4.9$, making the calorimeter system achieve its good hermeticity and minimizing the energy losses. It is assembled with tungsten rod absorbers embedded in a copper matrix. Between the two, a thin gap filled with liquid argon provides the active material.

2.2.5 Muon Spectrometers

The most external detector system is the muon spectrometer [13], a combination of toroidal superconducting magnets and precision chambers providing a measurement of the momentum of muons for $|\eta| < 2.7$. It is also equipped with an independent trigger system used for the first event triggering stage (see Sect. 2.4) active in the pseudorapidity region $|\eta| < 2.4$. Four subdetectors compose the muon system: Monitored Drift-Tube (MDT) chambers, Cathode Strips Chambers (CSC), Resistive Plate Chambers (RPC) and Thin Gap Chambers (TGC). The layout changes in the barrel and end-cap regions, and is schematically shown in Fig. 2.9. In the barrel region, chambers are arranged in three cylindrical layers around the beam axis, one layer being inside the magnet. In the end-caps these three layers are placed perpendicular

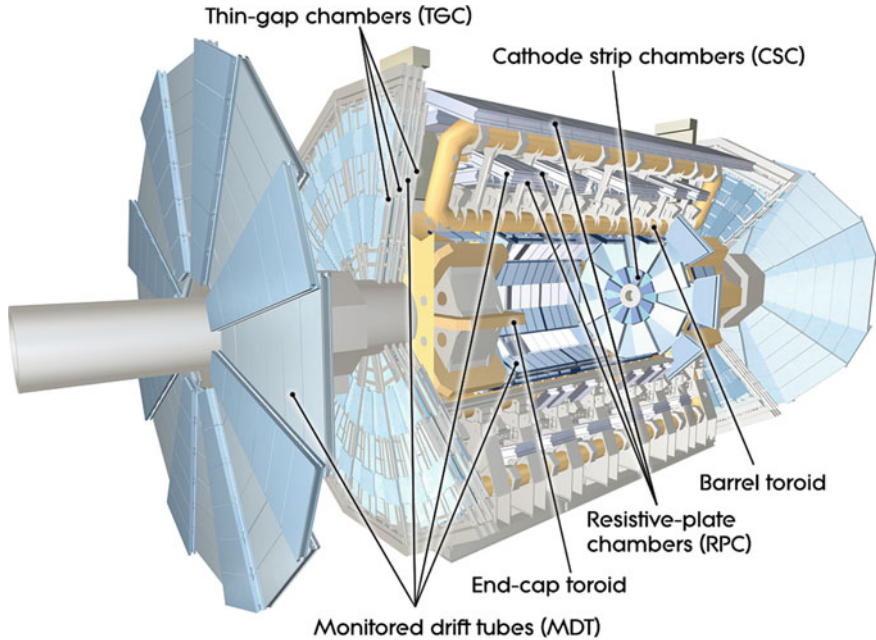


Fig. 2.9 Schematic view of the ATLAS muon spectrometer

to the beam axis. The variety of technologies used responds to the different needs of the detector (precise position and momentum measurement versus triggering and time measurement) and the large variation in particle flux from the central to the forward region.

2.2.5.1 Detection Chambers

MDT (Monitored Drift Tube chambers): MDTs are proportional chambers based on pressurized drift tubes filled with an argon and carbon dioxide mixture and with a tungsten-rhenium wire producing a radial electric field. Each chamber is composed of a group of six or eight tubes placed transverse to the beam axis. This number of tubes allows for a very good track reconstruction and high reduction of the fake tracks from random associations of background hits, providing a resolution on position of $80\ \mu\text{m}$ for an individual tube, $40\ \mu\text{m}$ for a chamber and $30\ \mu\text{m}$ for the three layers of MDTs. Due to their reliability, mechanical robustness and simpler operation, MDT chambers are employed to cover the larger area of the spectrometer ($|\eta| < 2.7, 2.0$ for the innermost layer).

CSC (Cathode Strip Chambers): CSCs are multiwire proportional chambers with wires oriented in the radial direction, spaced by $2.5\ \text{mm}$, and using the same gas mixture as the MDTs. CSCs are used at high pseudo-rapidities to help confront

the demanding rate and background conditions. The spacial resolution of the four layers of CSCs is $40\text{ }\mu\text{m}$ in the bending plane and 5 mm in the non-bending one. The maximum drift time for signal collection is 40 ns compared to the 700 ns of the MDTs, which gives the possibility to achieve higher acquisition rates. Due to this capability, together with the high radiation resistance, CSCs are used in the range $2.0 < |\eta| < 2.7$.

2.2.5.2 Triggering Chambers

For trigger purposes detectors with faster response than drift tubes are needed,⁴ MDTs and CSCs are therefore supplemented with special layers of triggering chambers.

RPC (Resistive Plate Chambers): RPCs are chambers with a gas mixture of $\text{C}_2\text{H}_2\text{F}_4$ (94.7 %), $\text{Iso-C}_4\text{H}_{10}$ (5 %) and SF_6 (0.3 %) between two resistive Bakelite plates. The avalanches are collected with two orthogonal sets of pick-up strips that provides a position resolution of 1 cm in each plane and 1 ns time resolution, allowing for individual bunch crossing discrimination. RPCs provide also the ϕ coordinate for the tracks in the final analysis, since MDTs only give the η coordinate.

TGC (Thin Gap Chamber): TGCs are multi-wire proportional chambers with the characteristic that the wire-to-cathode distance is smaller than the wire-to-wire distance for a fast collecting time. They are assembled in the end-cap wheels, covering the region $1.05 < |\eta| < 2.7$ (2.4 for triggering). The timing resolution is comparable to the RPC's one while the spatial resolution is in the range of $2\text{--}7\text{ mm}$ for both coordinates.

2.3 Forward Subdetectors and Luminosity Measurement

A good determination of the integrated luminosity is of particular importance to reach the ultimate precision in measurement of processes of interest. The luminosity, \mathcal{L} , defined in Eq. 2.1, can be rewritten as:

$$\mathcal{L} = \frac{\mu_{\text{vis}} n_b f_r}{\sigma_{\text{vis}}} , \quad (2.10)$$

where f_r is the collider revolution frequency, n_b the number of colliding bunches and σ_{vis} the visible inelastic cross section (total inelastic cross section times the detector acceptance and efficiency). The visible interaction rate per bunch crossing is denoted as μ_{vis} . It is extracted mainly from the signals coming from specific luminosity detectors. The simplest algorithm consists in “simple counting” of bunch

⁴Drift-time in tubes with a diameter of $\sim 10\text{ mm}$ can be of $\sim 500\text{ ns}$, too long with respect to the 25 ns spacing of the bunch crossings.

crossings where detectors reported a signal, but more refined algorithms [14] are used, in particular when the pile-up contamination is no longer negligible.

In order to use the measured μ_{vis} for luminosity determination, each detector and algorithm must be calibrated by determining its visible cross section σ_{vis} . The calibration technique exploits the *van der Meer* scans [15]. These are special low-intensity LHC runs where the beam separation in the transverse planes is varied (scanned) in order to determine the beams' overlap profile. Through the determination of the beam lateral profile the absolute luminosity of the particular run can be inferred using formula 2.1, and σ_{vis} can be determined for each subdetector.

ATLAS is supplemented with several detectors in the forward regions to perform luminosity measurements and monitoring. The main detectors for luminosity measurement are listed below:

LUCID (Luminosity measurements using Cherenkov Integrating Detector): a Cherenkov detector specifically designed for luminosity measurement. It consists of 16 aluminum tubes surrounding the beam pipe at 17 m from the interaction point. Each tube is filled with C_4F_{10} and is coupled to a photomultiplier in the back-end.

BCM (Beam Conditions Monitor): 1 cm^2 diamond detectors located at $z = \pm 184$ cm around the beam pipe. Their fast readout and good time resolution (0.7 ps) allow them to provide luminosity information for each bunch crossing. At the same time they are also employed to trigger on beam losses and induce the dump of the beam, thus protecting the silicon detectors from damage that might result from an uncontrolled beam.

ALFA (Absolute Luminosity For ATLAS): is a subdetector that is only activated during special runs. It consists of 8 scintillating fibers detectors placed at 240 m from the interaction point inside roman pots, above and below the beam pipe.

In addition, cross-checks of the luminosity measurement have been performed using information from other standard subdetectors: counting of primary vertices reconstructed by the ID and integrated signals from the Tile and forward calorimeter. The precision achieved is of a few % depending on the data-taking year.

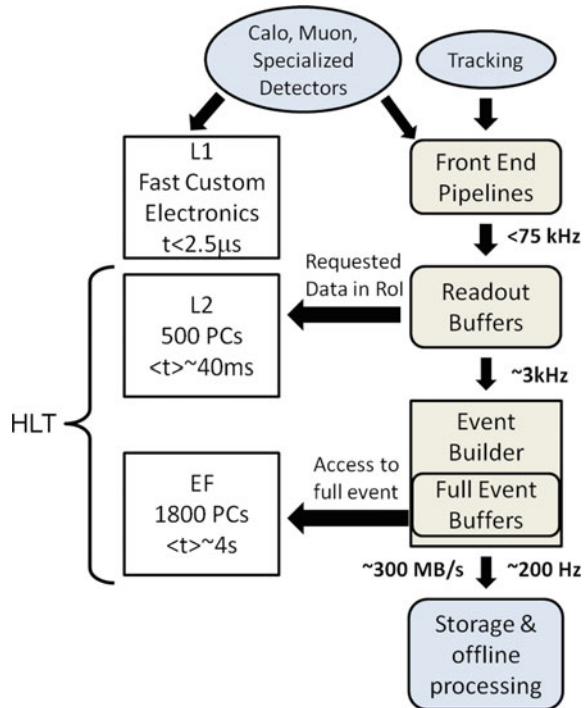
2.4 Trigger System

Due to technical limitations, not every LHC collision can be recorded by the ATLAS detector. The goal of the ATLAS trigger and data acquisition system is to select in real time events with interesting characteristics for physics analyses.

The ATLAS trigger system [16], shown schematically in Fig. 2.10, has a three-layer structure with increasingly detailed levels of information used in the reconstruction, and hence refinement of the selection criteria at each stage.

At the first stage, Level 1 (L1), hardware triggers use coarse calorimeter and muon information for the trigger decision. At this level the event rate is reduced

Fig. 2.10 Schema of the ATLAS trigger system



from 40 MHz (the frequency of the beam crossing) to a maximum of 75 kHz. In the cases where the trigger is passed, the L1 trigger defines one or more regions-of-interest (RoIs) in η and ϕ where the trigger has identified interesting features. The raw event data is then sent to the readout stream for the next trigger level.

The Level 2 (L2) trigger is based on software. At this stage the information from the trackers is incorporated to the RoI to build candidate objects (electrons, photons, muons) and their position and energy are computed. A tighter selection on these refined objects allows for a reduction of the throughput down to ≈ 3 kHz.

The final trigger level is the Event Filter (EF). The combination of the two software steps, L2 and EF, is referred to as High Level Trigger (HLT). At this point the physics objects are built using the same algorithms as the offline reconstruction. After the selection, the EF reduces the output rate to 200 Hz and the events are written to mass storage. Events passing the EF are assigned to streams defined to separate the events into different datasets for different analysis' interests, e.g. electron streams, muon streams, jet streams, etc.

Most of the trigger chains used for physics are un-scaled, meaning that all the events passing the selection are kept. Other trigger chains that contain either too many events or events considered not physically interesting are pre-scaled. These are characterized by a prescaling value, P , meaning that of all the events that activated

the trigger, only $1/P$ were accepted. These trigger chains are usually used for checks or calibration rather than physics analysis.

The term “trigger chain” refers to the sequence of selections that define a certain trigger object. The naming convention is:

$$[\text{LEVEL}][\text{N}][\text{TYPE(S)}][\text{THRESHOLD}][\text{ISOLATION}][\text{QUALITY}],$$

where the components, from left to right, are: the trigger level used, the multiplicity of the type, the object candidate, the threshold applied to the transverse momentum or energy of the object candidate, the object isolation and the severity of the final algorithm requirements.

Trigger chains define a *trigger menu*, where they are associated to their prescale value P , and which is chosen based on the physics program of the data-taking period, taking into account the LHC luminosity.

2.5 Data Quality

Not all collision events recorded by ATLAS are used for data analysis. Each sub-detector maintains a record of its performance across the run, and only the data collected with the subdetectors meeting certain quality requirements are considered for the analysis. Therefore, for each dataset Good Runs Lists (GRL) are compiled recording for each lumiblock⁵ which subdetectors satisfied the requirements. For the measurements presented in this dissertation, all ATLAS subsystems are needed, as the physics objects used in the analyses are reconstructed using the information from the full detector. The fraction of data considered as “good” is $\sim 95\%$, giving a total integrated luminosity of 20.3 fb^{-1} satisfying data quality that is used for these analyses.

References

1. ATLAS Collaboration (2012) Observation of a new particle in the search for the Standard Model Higgs boson with the ATLAS detector at the LHC. Phys Lett B 716:1. [arXiv:1207.7214](#) [hep-ex]
2. CMS Collaboration (2012) Observation of a new boson at a mass of 125 GeV with the CMS experiment at the LHC. Phys Lett B 716:30. [arXiv:1207.7235](#) [hep-ex]
3. Evans L, Bryant P, Machine LHC (2008) JINST 3:S08001
4. ALICE Collaboration (2008) The ALICE experiment at the CERN LHC. JINST 3:S08002
5. ATLAS Collaboration (2008) The ATLAS experiment at the CERN large hadron collider. JINST 3:S08003

⁵A luminosity block (lumiblock) is the smallest unit of time in the ATLAS data-taking defined as the minimal period where all the data-taking configurations are constant. In general the duration of a luminosity block is of the order of 1 min.

6. Collaboration CMS (2008) The CMS experiment at the CERN LHC. JINST 3:S08004
7. LHCb Collaboration (2008) The LHCb detector at the LHC. JINST 3:S08005
8. ATLAS Collaboration (1997) ATLAS: magnet system technical design report, CERN/LHCC/97-18
9. ATLAS Collaboration (1997) ATLAS: inner detector technical design report, CERN-LHCC-97-016/017
10. ATLAS Collaboration (2011) Studies of the performance of the ATLAS detector using cosmic-ray muons. Eur Phys J C 71:1593. [arXiv:1011.6665](#) [hep-ex]
11. ATLAS Collaboration (1996) ATLAS: liquid argon technical design report, CERN-LHCC-96-041
12. ATLAS Collaboration (1996) ATLAS: tile calorimeter technical design report, CERN/LHCC-96-042
13. ATLAS Collaboration (1997) ATLAS: muon spectrometer technical design report, CERN/LHCC-97-022
14. ATLAS Collaboration (2013) Improved luminosity determination in pp collisions at $\sqrt{s} = 7$ TeV using the ATLAS detector at the LHC, Eur Phys J C 73:2518. [arXiv:1302.4393](#) [hep-ex]
15. van der Meer S (1968) Calibration of the effective beam height in the ISR, CERN-ISR-PO-68-31
16. ATLAS Collaboration (1849) Performance of the ATLAS trigger System in 2010. Eur Phys J C 72:1849. [arXiv:1110.1530](#) [hep-ex]

Search for New Physics in $t\bar{t}$ Final States with
Additional Heavy-Flavor Jets with the ATLAS Detector

Montejo Berlingen, J.

2016, XIV, 283 p. 196 illus., 119 illus. in color.,

Hardcover

ISBN: 978-3-319-41050-0